BIOLOGICAL CRYSTALLOGRAPHY

ISSN 1399-0047

Combining 'dry' co-crystallization and *in situ* diffraction to facilitate ligand screening by X-ray crystallography

Muriel Gelin,[a,b] Vanessa Delfosse,[a,b] Frédéric Allemand,[a,b] François Hoh,[a,b] Yoann Sallaz-Damaz,[c,d,e] Michel Pirocchi,[c,d,e] William Bourguet,[a,b] Jean-Luc Ferrer,[c,d,e]* Gilles Labesse[a,b] and Jean-François Guichou[a,b]*

[a]CNRS, UMR5048 – Université de Montpellier, Centre de Biochimie Structurale, 34090 Montpellier, France, [b]INSERM, U1054, 34090 Montpellier, France, [c]Université Grenoble Alpes, IBS, 38044 Grenoble, France, [d]CNRS, IBS, 38044 Grenoble, France, and [e]CEA, IBS, 38044 Grenoble, France. *Correspondence e-mail: jean-luc.ferrer@ibs.fr, guichou@cbs.cnrs.fr

Received 29 January 2015
Accepted 29 May 2015

Edited by J. L. Martin, University of Queensland, Australia

Keywords: ligand screening; *in-situ* X-ray diffraction; fragment library screening; drug design; therapeutic targets.

PDB references: human nuclear receptor PPARγ, complex with rosiglitazone, 4xld; hen egg-white lysozyme, complex with benzamidine, 4xn6; human cyclophilin D, complex with ethyl 2-({[(4-aminophenyl)methyl]carbamoyl}amino)acetate, room temperature, 4xnc; 4zsc; 100 K, 3rdc; complex with 1-(4-aminobenzyl)-3-[4-(methylthio)-1-{2-[2-(methylthio)]-phenyl}pyrrolidin-1-yl)-1-oxobutan-2-yl]urea, 100 K, 4j5c; room temperature, 4zsd; Erk-2, complex with 1-phenyl-1*H*-1,2,4-triazole-3,5-diamine, room temperature, 4xne; 100 K, 4xp2; complex with 2-amino-6-thiopurine, room temperature, 4xoy; 100 K, 4xp3; complex with 1-*N*-{[3-(benzyloxy)phenyl]methyl}-2*H*-1,2,3,4-tetrazole-1,5-diamine, room temperature, 4xrj; 100 K, 4xoz; complex with 3-cyano-7-azaindole, room temperature, 4xrl; 100 K, 4xp0

X-ray crystallography is an established technique for ligand screening in fragment-based drug-design projects, but the required manual handling steps – soaking crystals with ligand and the subsequent harvesting – are tedious and limit the throughput of the process. Here, an alternative approach is reported: crystallization plates are pre-coated with potential binders prior to protein crystallization and X-ray diffraction is performed directly '*in situ*' (or in-plate). Its performance is demonstrated on distinct and relevant therapeutic targets currently being studied for ligand screening by X-ray crystallography using either a bending-magnet beamline or a rotating-anode generator. The possibility of using DMSO stock solutions of the ligands to be coated opens up a route to screening most chemical libraries.

1. Introduction

X-ray crystallography is now the method of choice to obtain structural information for biological macromolecules at high resolution. By mid-2014, 90 000 crystal structures had been deposited in the Protein Data Bank (PDB; http://www.rcsb.org/pdb; Rose *et al.*, 2011). In the field of rational drug design, X-ray crystallography is essential to precisely determine the mode of binding of known or potential binders, including weak binders, in order to guide lead optimization (Murray & Blundell, 2010). Indeed, fragment-based drug design has attracted great interest and has shown very promising results in recent years (Baker, 2013).

In the last two decades, major improvements have been achieved in sample production and crystallization as well as in X-ray sources, experimental setup and data processing (Cymborowski *et al.*, 2010). Automated crystallization assays are performed using dedicated robots and pre-established conditions. Nanodispensers have significantly improved the throughput of crystallogenesis by decreasing the amount of material needed. The use of these approaches is now widespread and routinely achieves high efficiency.

Until recently, handling and mounting macromolecular crystals to bring them into the X-ray beam has been a difficult or delicate step that has been performed manually. This important bottleneck has recently been resolved. Indeed, several approaches have been described to provide a more convenient way of bringing a crystal into an X-ray beam. They

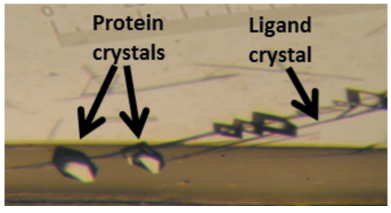

rely on growing crystals on supports that are directly amenable to *in situ* X-ray diffraction (Jacquamet *et al.*, 2004; Bingel-Erlenmeyer *et al.*, 2011; le Maire *et al.*, 2011) or to laser ablation prior to crystal cooling (Cipriani *et al.*, 2012), and more recently directly onto cryoloops (Yin *et al.*, 2014). The advantages are threefold: (i) rapid access to relevant diffraction information (crystal quality and an up to atomic resolution structure), (ii) the potential for complete automation and (iii) minimal manipulation of individual crystals to preserve crystal integrity prior to X-ray exposure.

All of the above developments significantly accelerate the determination of new macromolecular structures, even for membrane proteins (Axford *et al.*, 2015). This makes many new targets available for ligand screening. However, the addition of small chemical compounds remains a complex and tedious task whose automation is challenging. Indeed, some automation has been proposed and applied to two therapeutic targets (Davies *et al.*, 2009; Newman *et al.*, 2009). In one case, pre-coating crystallization plates with the desired ligands before or parallel to protein crystallization was devised, but only soaking was subsequently used (Davies *et al.*, 2009). In the second case, automatic addition of ligand was based on classical pipetting to add the ligand to preformed crystals (Newman *et al.*, 2009). Nevertheless, ligand soaking is still performed manually by the majority of crystallographers and novel approaches are necessary to address this problem. Three types of limitation might explain the limited success of the above two approaches. Firstly, we failed to reproduce efficient soaking using automatic pipetters, as in our cases the crystal crashed (dissolved or shattered) upon the addition of ligand solution. The alternative soaking by prior coating (as reviewed recently by Davies, 2014) still relies on protein crystal transfer onto pre-coated wells for ligand soaking. Thus, it requires physical manipulation of individual crystals, delicate and time-consuming addition of ligands, transfer of soaked crystals into cryoprotectants and cooling, all of which are steps that could potentially damage macromolecular crystals. Accordingly, macromolecule–ligand co-crystallization directly onto pre-coated wells represents an attractive alternative that could be tested. However, the use of methanol as a rapidly evaporating solvent makes the pipetting and storage of chemical compounds more complex (Davies, 2014) with, in addition, a mild toxicity issue.

Here, we describe the convenient combination of *in situ* diffraction and an optimized delivery of ligands prior to the crystallization step. It is based on coating the crystallization wells with the desired small molecules and allowing the solvent to evaporate prior to setting up protein crystallization in a classical way. To alleviate the problems of methanol use (toxicity and storage), we switched to DMSO as a more convenient solvent that is used in the vast majority of medicinal chemistry work. Furthermore, we have set up 'dry' co-crystallization directly in 96-well plates compatible with *in situ* diffraction. We tested this approach on several therapeutic targets as relevant test cases. Diffraction was performed using either an X-ray beam from a synchrotron source or a rotating-anode generator to collect data sets at room temperature. Evaluating the feasibility of recording the complete data set *in situ* using a rotating-anode source at a 1.54 Å wavelength was important as higher radiation damage can be expected during such experiments. Our results suggest that the combination of 'dry' co-crystallization and *in situ* diffraction can accelerate ligand screening by X-ray crystallography.

2. Materials and methods

2.1. Plate preparation for *in situ* ligand screening

Firstly, the evaporation behaviour of several solvents on 96-well CrystalQuick X plates (Greiner Bio-One) was tested. These crystallization plates possess an optimized geometry to allow *in situ* diffraction (le Maire *et al.*, 2011). Various volumes (0.2, 0.5 and 1.0 µl) of the desired solvent were dispensed into the square drop wells and left to evaporate. The evaporation was monitored by visual survey. It appeared that at least 1 µl was necessary to fully cover the bottom of the drop well and to make sure that the ligand would be deposited over the whole surface. Accordingly, all of the following experiments were performed using this volume for ligand deposition.

For ligand screening, stock solutions of chemical compounds were prepared in DMSO or ultrapure water at a concentration of 10 m*M*. Plates were pre-coated by dispensing 1 µl ligand solution into each well using an automatic nanolitre dispenser (Cartesian HoneyBee X8; Genomic Solutions Inc.). The same ligand was dispensed along a 12-well row to ensure that sufficient crystals could be grown and tested. The plates were then left under the laboratory hood for one week to eliminate DMSO or water solvent while being protected with filter paper to prevent dust from entering the well.

Crystallization drops were prepared with crystallization robots. The wells were filled with 40 µl crystallization buffer, and 500 nl of the reservoir was mixed with 500 nl of the protein sample prior to deposition at the drop location. The plate was then sealed with a transparent plastic film (Greiner G-676070) and kept at 18°C until beam time was made available.

2.2. Protein expression, purification and crystallization

For the tests, we used three well behaved proteins previously studied in the laboratory (see below) and one other protein frequently used as gold standard in the field of X-ray crystallography (hen egg-white lysozyme). They readily crystallize and diffract well. Furthermore, we took advantage of the different space groups (*i.e.* monoclinic and tetragonal) to evaluate the limits of the currently available range of orientation angles for the plates.

2.2.1. Hen egg-white lysozyme. Lysozyme was purchased from Sigma (catalogue No. L6876) and was dissolved in ultrapure water at a concentration of 120 mg ml^{-1} and then filtered through a 0.22 µm filter. Lysozyme crystals were grown using the sitting-drop vapour-diffusion method at 18°C in the pre-coated plates. Drops were formed by mixing 0.5 µl protein solution with an equal volume of mother liquor consisting of 100 m*M* sodium acetate pH 4.6, 4%(*w*/*v*) NaCl and were

Table 1
Crystallographic data-collection and refinement statistics.

Values in parentheses are for the highest resolution shell.

Protein ID	Lysozyme	CypD	CypD	CypD	CypD	CypD	PPARγ
Ligand	BAM	EA4	EA4	EA4	7I6	7I6	BRL
Data collection							
Crystal mouting	*In situ*	*In situ*	*In situ*	Cryoloop	*In situ*	Cryoloop	*In situ*
Beamline	BM30A	In-house	BM30A	In-house	BM30A	ID29	BM30A
Wavelength (Å)	0.9797	1.542	0.9797	1.542	0.97922	0.9793	0.9797
Temperature (K)	298	298	298	100	298	100	298
Space group	$P4_32_12$	$P4_12_12$	$P4_12_12$	$P4_12_12$	$P4_12_12$	$P4_12_12$	$P4_32_12$
Unit-cell parameters							
a (Å)	79.3	57.9	57.9	56.4	57.9	57.3	66.9
b (Å)	79.3	57.9	57.9	56.4	57.9	57.3	66.9
c (Å)	38.1	88.5	88.5	87.0	88.6	87.5	157.4
$\alpha = \beta = \gamma$ (°)	90.0	90.0	90.0	90.0	90.0	90.0	90.0
Resolution (Å)	38.1–1.35	29.5–2.23	48.4–1.50	28.2–1.93	48.5–1.45	48.0–1.03	47.4–2.45
R_{sym} or R_{merge}	0.090 (0.280)	0.052 (0.121)	0.047 (0.228)	0.031 (0.188)	0.102 (0.412)	0.087 (0.216)	0.154 (0.477)
$\langle I/\sigma(I)\rangle$	2.5 (1.6)	18.8 (11.5)	12.1 (3.5)	9.1 (3.5)	7.0 (2.5)	18.8 (3.9)	7.4 (4.7)
Completeness (%)	99.5 (98.9)	98.1 (99.6)	73.1 (78.5)	97.5 (84.0)	99.2 (93.9)	96.9 (79.4)	90.0 (77.8)
Multiplicity	4.3 (3.9)	4.5 (4.3)	2.8 (2.6)	4.1 (4.8)	2.0 (1.8)	10.5 (3.3)	4.4 (3.7)
Wilson B (Å^2)	12.4	14.0	5.2	13.2	8.6	7.7	41.1
No. of crystals†	1	2/3	1	1	1	1	1/2
Refinement							
No. of reflections	21988	6820	16982	10358	25914	32279	12485
R_{work}/R_{free} (%)	13.8/16.5	17.9/23.8	13.4/16.5	20.8/27.0	13.4/15.5	12.3/16.2	19.3/22.2
No. of atoms							
Protein	1072	1245	1260	1232	1256	1302	2053
Ligand	9	18	18	18	32	32	28
Water	95	65	91	223	106	463	25
B factors (Å^2)							
Protein	16.6	17.1	9.6	15.8	11.9	12.2	44.6
Ligand	18.7	15.1	10.2	17.5	19.9	14.9	58.1
Water	29.5	22.6	19.8	24.1	25.5	23.8	41.3
R.m.s.d., bond (Å)	0.007	0.009	0.007	0.007	0.007	0.011	0.004
R.m.s.d., angles (°)	1.239	1.321	1.300	1.470	1.303	1.660	0.799
PDB code	4xn6	4xnc	4zsc	3rdc	4zsd	4j5c	4xld

† The first number is the number of crystals used to solve the structure and the second number is the number of crystals collected.

equilibrated over 40 µl of the same solution. Crystals formed in about 1–2 d.

2.2.2. Human cyclophilin D K175I mutant. Purification of the K175I mutant of human cyclophilin D (CypD) was performed as described previously (le Maire *et al.*, 2011). CypD K175I crystals were grown using the sitting-drop vapour-diffusion method at 18°C in the pre-coated plates. Drops were formed by mixing 0.5 µl protein solution with an equal volume of mother liquor consisting of 25%(*w*/*v*) PEG 4000 and were equilibrated over 40 µl of the same solution. Crystals formed overnight. The crystallization procedure was optimized by the seeding method using the Seed Bead protocol (Hampton Research). A stock solution for seeding was prepared from one crystal vortexed in a microcentrifuge tube with 500 µl reservoir solution. Serial dilutions were prepared and the optimal dilution was determined by trial assays. For data collection at 100 K, crystals were cryoprotected by brief immersion in oil.

2.2.3. Human wild-type PPARγ LBD. Wild-type PPARγ LBD (Gln203–Tyr477) was cloned into the pET-15b vector. Gene expression was induced in *Escherichia coli* BL21 (DE3) cells overnight at 20°C in LB medium without any ligand and the protein was purified in the apo form. The cell lysate (in 20 m*M* Tris pH 8.0, 500 m*M* NaCl) was first applied onto a nickel affinity column (HiTrap 5 ml; GE Healthcare). The eluted protein was further purified by size-exclusion chromatography (Superdex 75 HR 26/60; GE Healthcare) and was then concentrated to 4.5 mg ml^{-1} and stored at 40°C in gel-filtration buffer (20 m*M* Tris pH 8.0, 150 m*M* NaCl, 5 m*M* DTT, 10% glycerol). Crystals were obtained in 3–4 *M* sodium formate pH 7–7.5. Crystals formed in about 1–2 d (Zhang *et al.*, 2011).

2.2.4. Rat ERK2. The overproduction and purification of rat Erk2 protein were performed using standard protocols as described previously (le Maire *et al.*, 2011). Erk2 crystals were grown in the pre-coated plates using the sitting-drop vapour-diffusion method at 18°C. Drops were formed by mixing 0.5 µl protein solution with an equal volume of mother liquor consisting of 100 m*M* MES pH 6.5, 200 m*M* ammonium sulfate, 20 m*M* β-mercaptoethanol, 26%(*w*/*v*) PEG MME 2000 and were equilibrated over 40 µl of the same solution. Crystals formed in about 3–6 d. The crystallization procedure was optimized by the seeding method using the Seed Bead protocol as in the case of CypD (see above). For cryo data collection, crystals were cryoprotected by brief immersion in oil.

Table 2
Crystallographic data-collection and refinement statistics.

Values in parentheses are for the highest resolution shell.

Protein ID	Erk2	Erk2	Erk2	Erk2	Erk2	Erk2
Ligand	**1**	**1**	**1**	**2**	**2**	**2**
Data collection						
Crystal mouting	*In situ*	*In situ*	Cryoloop	*In situ*	*In situ*	Cryoloop
Beamline	BM30A	In-house	In-house	BM30A	In-house	BM30A
Wavelength (Å)	0.97922	1.542	1.542	0.97970	1.542	0.97970
Temperature (K)	298	298	100	298	298	100
Space group	$P2_1$	$P2_1$	$P2_1$	$P2_1$	$P2_1$	$P2_1$
Unit-cell parameters						
a (Å)	49.3	49.3	48.7	49.1	49.3	48.6
b (Å)	71.4	71.6	70.3	71.6	71.7	70.3
c (Å)	61.3	61.1	59.9	60.9	61.0	59.8
$\alpha = \gamma$ (°)	90.0	90.0	90.0	90.0	90.0	90.0
β (°)	109.5	109.0	109.0	109.1	109.1	108.9
Resolution (Å)	29.3–2.10	28.4–2.30	56.6–1.78	44.8–1.80	29.3–2.22	28.5–1.74
R_{sym} or R_{merge}	0.126 (0.513)	0.100 (0.347)	0.037 (0.149)	0.149 (0.579)	0.110 (0.317)	0.035 (0.289)
$\langle I/\sigma(I)\rangle$	6.0 (1.9)	7.5 (2.9)	9.1 (5.0)	6.8 (2.5)	8.8 (4.3)	11.9 (1.4)
Completeness (%)	89.8 (67.9)	87.1 (86.9)	95.1 (79.9)	97.3 (99.0)	87.9 (84.7)	89.7 (89.6)
Multiplicity	2.5 (2.6)	2.5 (2.3)	2.0 (1.8)	2.9 (2.8)	2.9 (3.0)	1.8 (1.8)
Wilson B (Å^2)	29.8	33.5	19.0	28.2	30.7	24.9
No. of crystals†	2/9	8/8	1	4/7	6/7	1
Refinement						
No. of reflections	21139	14977	34518	34272	16041	34736
R_{work}/R_{free} (%)	18.2/22.1	17.9/23.8	14.9/17.9	17.8/21.8	17.9/23.8	18.5/22.6
No. of atoms						
Protein	2739	2818	2912	2887	2818	2832
Ligand	11	11	11	13	13	13
Water	122	39	460	126	55	273
B factors (Å^2)						
Protein	37.7	40.4	20.7	33.7	38.0	28.1
Ligand	30.3	43.2	28.5	38.0	34.1	43.4
Water	43.3	33.1	37.2	36.6	32.9	35.6
R.m..s.d., bonds (Å)	0.009	0.009	0.009	0.010	0.009	0.008
R.m..s.d., angles (°)	1.175	1.356	1.021	1.417	1.412	0.951
PDB code	4xoy	—	4xp3	4xne	—	4xp2

† The first number is the number of crystals used to solve the structure and the second number is the number of crystals collected.

2.3. Data collection and processing

Data were collected from the cooled crystals on the FIP-BM30A, ID14-2, ID23-2 and ID29 beamlines at the ESRF, Grenoble, France or, in a few cases, on a MicroMax-007 HF rotating-anode generator (Rigaku) equipped with a focusing mirror (Osmic Inc.) and a MAR345 image-plate detector (MAR Research Inc.). For *in situ* diffraction, we recorded data on either FIP-BM30A or on a rotating-anode generator equipped with a G-Rob system (NatX-ray SAS) and a CCD camera (Photonics Inc.). In the case of *in situ* diffraction, dataset merging was performed 'on-the-fly' and data collections were continued until an acceptable completeness was achieved.

Data processing was performed using *iMosflm* (Powell *et al.*, 2013) or *XDS* (Kabsch, 2010) and *SCALA* from the *CCP*4 suite (Winn *et al.*, 2011). Structure refinement was performed using *REFMAC*5 (Murshudov *et al.*, 2011) or *PHENIX* (Adams *et al.*, 2010) and model building was performed with *Coot* (Emsley *et al.*, 2010). The files for all chemical compounds (PDB and CIF) were generated using *eLBOW* (Moriarty *et al.*, 2009) and *PRODRG* (Schüttelkopf & van Aalten, 2004). Figures were generated using *PyMOL* (http://www.pymol.org).

2.4. PDB accession codes

The Protein Data Bank accession codes for the coordinates of the complexes reported in this paper (see Tables 1, 2 and 3) are as follows: lysozyme with benzamidine (BAM) at 298 K, 4xn6; CypD with ethyl 2-({[(4-aminophenyl)methyl]-carbamoyl}amino)acetate (EA4) at 298 K, 4xnc and 4zsc, and at 100 K, 3rdc; CypD with 1-(4-aminobenzyl)-3-[4-(methylthio)-1-{2-[2-(methylthio)phenyl]pyrrolidin-1-yl}-1-oxobutan-2-yl]urea (7I6) at 298 K, 4zsd, and at 100 K, 4j5c; PPARγ LBD with rosiglitazone (BRL) at 298 K, 4xld; Erk2 with 2-amino-6-thiopurine (**1**) at 298 K, 4xoy, and at 100 K, 4xp3; Erk2 with 2,5-diaminophenyltriazole (**2**) at 298 K, 4xne, and at 100 K, 4xp2; Erk2 with 7-cyano-7-azaindole (**3**) at 298 K, 4xrl, and at 100 K, 4xp0; Erk2 with 1-*N*-{[3-(benzyloxy)phenyl]methyl}-2*H*-1,2,3,4-tetrazole-1,5-diamine (**4**) at 298 K, 4xrj, and at 100 K, 4xoz.

2.5. Affinity measurements

Affinities of the fragments for CypD or Erk-2 were derived from thermal shift assays or from enzymatic measurements. Thermal shift assays were set up using SYPRO Orange and fluorescence was monitored on a plate reader (QPCR Agilent

Table 3
Crystallographic data-collection and refinement statistics.

Values in parentheses are for the highest resolution shell.

Protein ID	Erk2	Erk2	Erk2	Erk2	Erk2
Ligand	**3**	**3**	**4**	**4**	**4**
Data collection					
Crystal mouting	*In situ*	Cryoloop	*In situ*	*In situ*	Cryoloop
Beamline	In-house	ID23-2	BM30A	In-house	ID14-2
Wavelength (Å)	1.542	0.8726	0.97970	1.542	0.93300
Temperature (K)	298	100	298	298	100
Space group	$P2_1$	$P2_1$	$P2_1$	$P2_1$	$P2_1$
Unit-cell parameters					
a (Å)	48.5	48.9	49.1	49.2	49.2
b (Å)	70.8	70.8	71.5	71.5	71.6
c (Å)	60.5	60.4	60.8	60.9	60.9
$\alpha = \gamma$ (°)	90.0	90.0	90.0	90.0	90.0
β (°)	109.5	109.0	108.7	108.7	108.7
Resolution (Å)	30.1–2.55	28.9–1.46	44.8–1.69	29.1–2.23	31.6–1.95
R_{sym} or R_{merge}	0.076 (0.337)	0.031 (0.480)	0.077 (0.339)	0.102 (0.363)	0.023 (0.209)
$\langle I/\sigma(I)\rangle$	7.6 (3.2)	9.5 (1.3)	3.6 (2.1)	8.7 (3.3)	13.5 (2.3)
Completeness (%)	88.2 (66.4)	95.4 (85.7)	93.0 (92.4)	92.8 (92.1)	93.1 (75.2)
Multiplicity	1.8 (1.8)	2.2 (2.2)	3.0 (2.8)	2.6 (2.4)	2.6 (2.4)
Wilson B (Å^2)	36.8	20.1	16.9	28.3	27.6
No. of crystals†	2/4	1	2/4	6/7	1
Refinement					
No. of reflections	10787	64302	39592	14722	27176
R_{work}/R_{free} (%)	17.9/22.8	19.0/21.4	13.6/18.0	16.0/20.8	14.5/18.8
No. of atoms					
Protein	2770	2899	2980	2919	2831
Ligand	11	11	22	22	22
Water	44	356	161	111	141
B factors (Å^2)					
Protein	42.3	25.8	27.6	33.6	35.6
Ligand	48.9	30.7	20.3	23.6	37.0
Water	36.9	37.3	35.7	33.2	43.1
R.m.s.d., bonds (Å)	0.009	0.014	0.012	0.011	0.012
R.m.s.d., angles (°)	1.214	1.100	1.456	1.291	1.424
PDB code	4xrl	4xp0	4xrj	—	4xoz

† The first number is the number of crystals used to solve the structure and the second number is the number of crystals collected.

Mx3005P). In a 96-well white quantitative PCR low-profile plate, 39 µl of a solution consisting of a 1:1 volume ratio of protein and SYPRO Orange dye (1:500 dilution) was dispensed and 1 µl of the desired ligand in DMSO was added. Ligands were generally tested at 100, 500 and 1 m*M* and protein at 2–4 µ*M*. The plate was sealed with an optical PCR seal and smoothly spun before being placed in the PCR instrument, where the temperature was increased from 25 to 95°C at 1°C min^{-1} while the fluorescence was monitored. Data were analyzed and T_m was determined by fitting to the Boltzmann equation using *GraphPad Prism* 5. Finally, ΔT_m was calculated using the T_m value from DMSO without ligand as a reference.

Inhibition at one concentration was measured at 1 m*M* in the case of CypD (Kofron *et al.*, 1991) and at 0.1 m*M* for Erk-2 (subcontracted to ReactionBiology).

3. Results

3.1. Ligand deposition

Firstly, we searched for a solvent that provides efficient solubilization of various chemical compounds and optimal evaporation while being compatible with the plate polymer (here a cyclic olefin copolymer). Methanol has previously been used for pre-coating ligands onto crystallization plates, but its use suffered from several drawbacks (Davies, 2014). Following this example, we tested rapidly evaporating solvents such as acetone, tetrahydrofuran, ethanol and acetonitrile. However, these solvents rapidly wicked out of the drop well, preventing proper coating. Among the other organic solvents that we tested (DMSO, 2-propanol and also water), only water and DMSO behaved adequately. Although it is slowly evaporating, DMSO was selected because it is the most versatile solvent and provides access to most chemical libraries. Drying was left to occur for one week before crystallization of the desired protein was set up in a classical way using the crystal-growth conditions previously established for the protein (Fig. 1*a*). In the following examples, crystallization was performed in conditions almost identical to those previously described in the literature apart from the systematic use of microseeding to enhance the reproducibility of the crystallization.

The affinity of fragments usually ranges from micromolar to ten-millimolar and hence requires a high compound concentration to achieve full occupancy of the protein binding site.

Here, fragments were all added at a concentration of 10 m*M* in 1 µl (but higher concentrations may be used). Thus, the highest ligand concentration may reach 20 m*M* after complete re-solubilization in the equilibrated crystallization drops. Notably, all of the ligands described below (except for benzamidine) are soluble in 100% DMSO but not in water, while their solubility in the mother liquors is unknown but is likely to be very low.

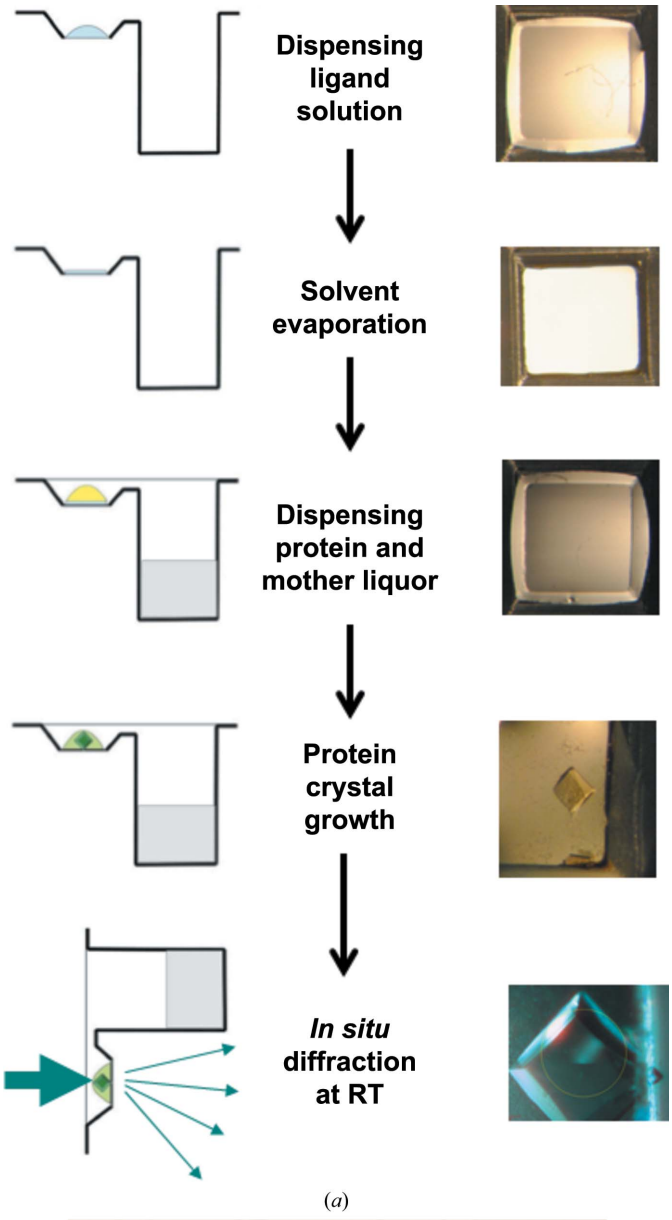

Figure 1
Soaking strategy. (*a*) The steps for 'dry' co-crystallization and *in situ* X-ray crystallographic screening are shown. Pre-coating of chemical compounds is first performed with a liquid dispenser. The solvent is evaporated gently before protein crystallization is set up. The protein crystal can then be harvested or *in situ* diffraction can be performed. (*b*) Enlargement of a drop containing crystals of Erk2 protein and ligand **3**.

3.2. Validating test cases

Firstly, we checked the feasibility of pre-coating crystallization plates using a water-soluble compound recently shown to bind to the surface of lysozyme (Yin *et al.*, 2014). Success with this example then prompted us to evaluate this new approach on therapeutic targets crystallizing in different conditions, in low- or high-symmetry lattices and belonging to distinct protein families.

3.2.1. Lysozyme and water-soluble benzamidine. As a first test case, we used hen egg-white lysozyme to compare our approach with a recently published approach (Yin *et al.*, 2014) that relies on building up co-crystallization drops directly onto cryoloops. In the present study, benzamidine (molecular weight 120, *X*log*P* 1.63) was solubilized in water, deposited on the well bottom and allowed to dry before crystallization of lysozyme was performed. Using *in situ* diffraction on one single crystal and at room temperature (RT), a complete data set was collected to 1.35 Å resolution on the bending-magnet beamline BM30A. Standard refinement rapidly led to excellent statistics (R_{work} = 13.8%, R_{free} = 16.5%; Table 1). The deduced structure (Supplementary Fig. S1) perfectly matched that previously described for the benzamidine-bound lysozyme complex (PDB entry 4n8z; Yin *et al.*, 2014). The weak binder (in the millimolar range) was detected at the same position with 70% occupancy (compared with 100% in the cooled structure) and a low *B* factor (18.7 *versus* 16.7 Å^2). This result suggests that water-soluble fragments can be readily screened using pre-coating and efficiently detected using *in situ* diffraction. We also tested *N*-acetylglucosamine (molecular weight 251, *X*log*P* −2.19) as a potential low-affinity fragment binding into the active-site groove. However, in our conditions we could not detect binding to the crystallized lysozyme (data not shown), while binding has been detected by others (Tanley *et al.*, 2012) but at much higher concentrations (150–250 m*M*).

3.2.2. Co-crystal of cyclophilin D with one fragment and one lead compound. Human cyclophilin D (CypD) belongs to the proline isomerase family. It is a validated target in ischaemia (Alam *et al.*, 2015) for which we have previously performed a fragment-screening campaign (Guichou *et al.*, 2011). We attempted to partially reproduce this screen using 'dry' co-crystallization and *in situ* diffraction. CypD crystallization was set up in two 96-well plates with a total of nine chemical compounds (one per row). A sufficiently large number (4–12) of crystals was obtained for only four fragments during this focused screening campaign. Despite decent diffraction that could be recorded from most of the crystals grown, only one complex could be detected.

Three fragments (*X*log*P* ranging from 0.1 to 1.3 and molecular weight ranging from 133 to 156) have been observed previously in cooled crystals (see PDB entries 3r4g, 3r57 and 3r56), but we could not detect their binding by precoating followed by *in situ* diffraction. These results may be explained by the low solubility of these compounds and their very low affinity for the target. Indeed, they showed weak inhibition (from 17 to 39%) at a concentration of 1 m*M*, while successful soaking relied on solubilizing these fragments in the cryoprotecting oil (to be described in further detail elsewhere).

Nevertheless, from the various fragments detected in the previous screen (Guichou *et al.*, 2011) we could build up a more elaborate fragment, ethyl 2-({[(4-aminophenyl)methyl]-carbamoyl}amino)acetate (Fig. 2*a*), which is poorly soluble in water (molecular weight 251, *X*log*P* 0.37) but displays micromolar affinity for this cyclophilin (Guichou *et al.*, 2011).

Three crystals were exposed to the X-ray beam directly 'in plate' at RT on the rotating-anode generator. 1° oscillation images were acquired in 1 min on the rotating-anode generator, and no radiation damage was detected during the time of acquisition. These crystals diffracted well and were isomorphous to that of the apo form reported previously (le Maire *et al.*, 2011). Thanks to the high-symmetry space group ($P4_12_12$), a very complete data set (98%) could be recorded from only two crystals with good multiplicity (4.5) at 2.23 Å resolution (Table 1). The resolution is currently limited by the CCD camera, as indicated by the high intensity in the outer shell [$I/\sigma(I)$ = 11.5]. This excellent statistic should allow follow-up studies (for example, molecular dynamics at RT), while the data set from the single best crystal reached 92% completeness and would have been sufficient to characterize the mode of binding of the ligand. Indeed, one crystal was exposed at RT on the bending-magnet beamline BM30A. A less complete data set (73.1%) was recorded to a high resolution of 1.50 Å but was sufficient to detect ligand binding (see below). In parallel, manual ligand soaking was performed on apo-form crystals, which were cooled to 100 K before data collection using a classical protocol on the same laboratory rotating-anode generator. In this case only one crystal was used to collect data to 1.93 Å resolution with otherwise similar statistics (Table 1).

In all cases, after isomorphous replacement using the apo structure a clear extra density was detected showing that the ligand could be readily detected. Refinement was straightforward in all cases and led to molecular models showing very good statistics (Table 1). The inhibitor adopted the same mode of binding at RT and at 100 K (Figs. 2*c*, 2*d* and 2*e*). Final refinement highlighted 100% occupancy and a low *B* factor (at RT; 15.1 and 10.2 Å^2 *versus* 17.5 Å^2 for the cryo structure) for the ligand in the structures.

In order to better characterize the mechanism in the 'dry' crystallization process (co-crystallization *versus* soaking), we selected a second compound, 1-(4-aminobenzyl)-3-(4-methyl-1-{2-[2-(methylthio)phenyl]pyrrolidin-1-yl}-1-oxopentan-2-yl)-urea (Supplementary Fig. S2*a*), which is poorly soluble in water (molecular weight 454, *X*log*P* 3.14) but displays a submicromolar affinity for CypD (Guichou *et al.*, 2011), as this particular complex could only be obtained by a co-crystallization experiment.

Firstly, we attempted a long soaking experiment (one week) on an apo crystal of CypD to obtain the complex. We collected data from three cooled crystals on a cryoloop at high resolution (between 1.1 and 1.4 Å); none gave an extra density for the ligand. Secondly, we used a co-crystallization experiment to collect a data set (at a high resolution of 1.03 Å) and a clear density was observed (Supplementary Figs. S2*b* and S2*c*),

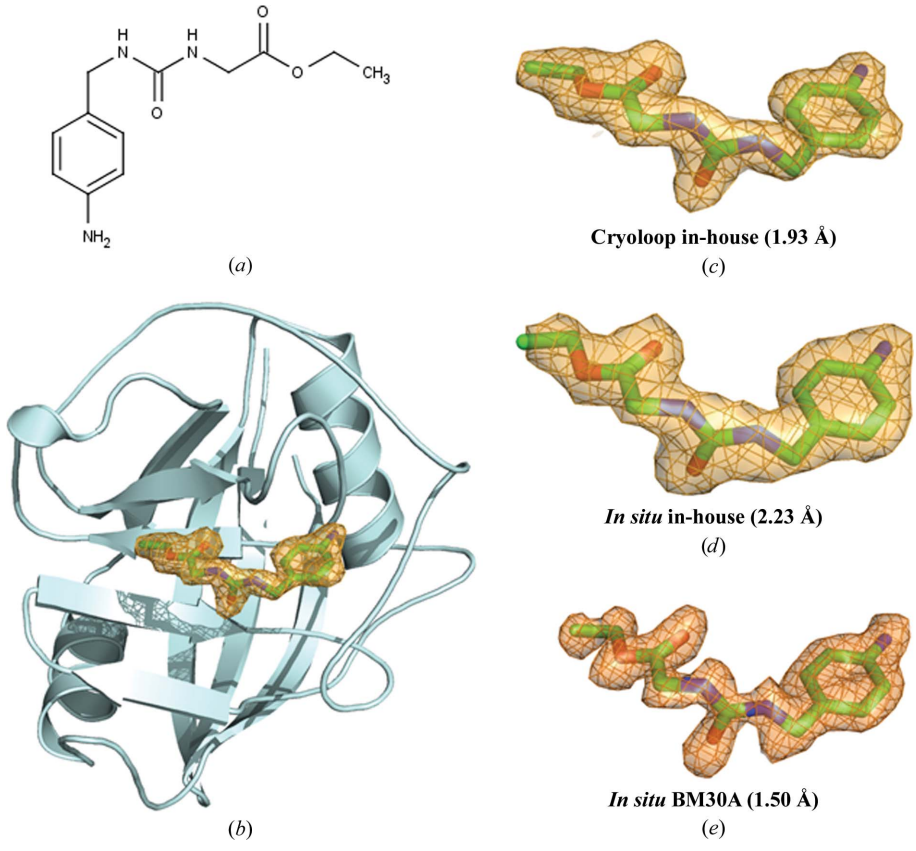

Figure 2
Crystal structures of the human prolyl isomerase cyclophilin D in complex with ethyl 2-({[(4-aminophenyl)methyl]carbamoyl}amino)acetate. (*a*) Chemical structure of ethyl 2-({[(4-aminophenyl)methyl]carbamoyl}amino)acetate. (*b*) The overall structure of cyclophilin D shown as a cartoon representation. (*c*) Structure solved at high resolution at 100 K. (*d*) The same structure at RT using data collected on a rotating-anode generator. (*e*) The same structure at RT using data collected on the synchrotron beamline BM30A at ESRF. In all panels, the $2F_o - F_c$ electron-density map (contoured at 1σ) was computed with the ligand molecule omitted in the Fourier synthesis.

allowing the ligand to be placed to yield a final refinement with excellent statistics (Table 1). Finally, using *in situ* diffraction on one single crystal and at RT, a complete data set (99.2%) was collected at 1.45 Å resolution on the bending-magnet beamline BM30A. Again, a clear extra density was detected, showing that the compound could be readily detected. Refinement was performed and led to a molecular model with very good statistics (Table 1). The inhibitor adopted the same mode of binding at RT and at 100 K (Supplementary Figs. S2*c* and S2*d*), although with a lower occupancy (70 *versus* 100%, respectively), and had low *B* factors (19.9 *versus* 14.9 Å^2). This result suggests that the 'dry' crystallization technique proceeds through co-crystallization.

3.2.3. Co-crystal of a nuclear receptor (PPARγ) with rosiglitazone. The human peroxisome proliferator-activated receptor γ (PPARγ) belongs to the PPAR nuclear hormone receptor subfamily, which controls the expression of genes involved in adipogenesis, glucose, lipid and cholesterol metabolism (Michalik *et al.*, 2006; Varga *et al.*, 2011). PPARγ is highly expressed in adipose tissues and plays key roles in regulating adipogenesis (Tontonoz & Spiegelman, 2008), lipid metabolism and glucose homeostasis through the improvement of insulin sensitivity (Ahmadian *et al.*, 2013). Thus, PPARγ is a target for antidiabetic agents of the thiazolidinedione class, which include troglitazone, pioglitazone and rosiglitazone. Co-crystallization of the LBD domain of PPARγ with a nanomolar agonist, rosiglitazone [5-({4-[2-(methylpyridin-2-ylamino)-ethoxy]phenyl}methyl)-1,3-thiazolidine-2,4-dione; molecular weight 357, *X*log*P* 2.64], was readily obtained by plate precoating using DMSO solution and crystallization conditions previously described for this protein (Zhang *et al.*, 2011). In this case, the crystals were less well diffracting and data collection was performed on the synchrotron beamline BM30A. Thanks to the high-symmetry space group ($P4_32_12$), one crystal was sufficient to record a complete data set at 2.45 Å resolution with very good multiplicity (Table 1). Standard refinement from the apo form rapidly led to extra electron density in the ligand-binding pocket in which we could recognize the rosiglitazone (Supplementary Fig. S3). The refined structure (R_{work} = 18.5%, R_{free} = 23.9%) perfectly matched the previously described complex (PDB entry 2prg) solved at 2.3 Å resolution (Nolte *et al.*, 1998). This demonstrated the feasibility of streamlining ligand screening on this important family of therapeutic targets harbouring a deeply buried ligand-binding pocket. This result is of importance as nuclear receptors are the targets of about 20% of currently used drugs and of numerous environmental pollutants (Delfosse *et al.*, 2012), the mode of binding of which still has to be deciphered for the vast majority.

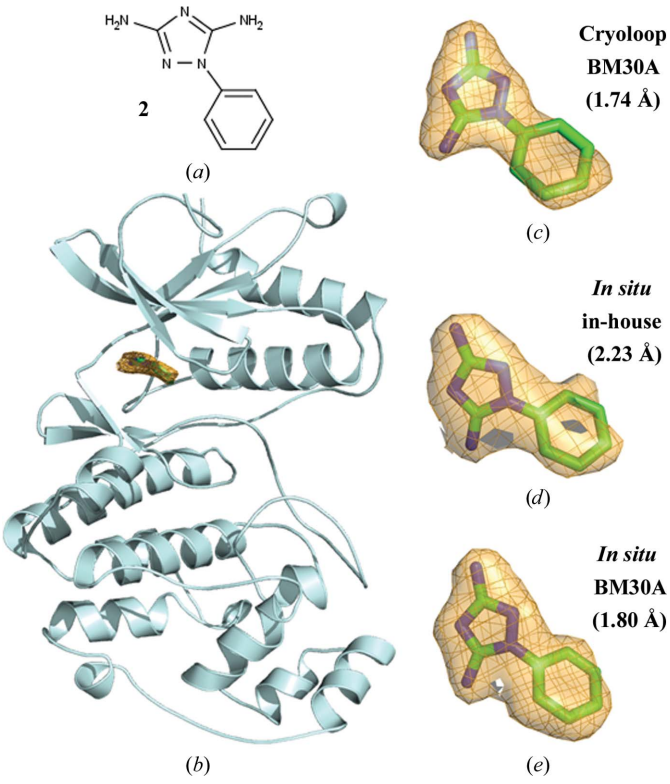

Figure 3
Crystal structures of the protein kinase Erk-2 in complex with 1-phenyl-1*H*-1,2,4-triazole-3,5-diamine (**2**). (*a*) Chemical structure of compound **2**. (*b*) The overall structure of Erk-2 shown as a cartoon representation. (*c*) Structure solved at high resolution at 100 K. (*d*) The same structure at RT using data collected on a rotating-anode generator. (*e*) The same structure at RT using data collected on the synchrotron beamline BM30A at ESRF. In all panels the $2F_o - F_c$ electron-density map (contoured at 1σ) was computed with the ligand molecule omitted in the Fourier synthesis.

3.2.4. Ligand screening on a challenging low-symmetry test case: Erk-2. A typical MAP kinase, Erk-2 is involved in numerous and important signalling pathways and its misfunction is linked to several diseases, including inflammation and cancer (Wortzel & Seger, 2011). As such, it is an important therapeutic target, but it still lacks a drug compound for clinical use. Here, we developed a screen with the rat protein kinase Erk-2 as a surrogate for the human orthologue. Crystals of rat Erk-2 are easily reproducible and usually diffract well. Nevertheless, their low-symmetry space group ($P2_1$) represents a severe challenge for the collection of a complete data set *in situ* owing to geometric constraints (le Maire *et al.*, 2011). We tested the feasibility of ligand screening on the rat protein kinase Erk-2 using 14 chemical compounds which are poorly soluble in water. Co-crystallization was set up in four plates with one ligand per row (some in duplicate). For nine ligands no crystal grew and in one case they were too small to diffract. For the remaining four fragments, a sufficient number of drops (4–12) yielded sufficiently large crystals to measure decent diffraction. Fortunately, in these four cases ligand binding could be detected. To our knowledge, no crystal structure of any protein kinase has been reported in complex with any of these four compounds. These molecules harbour privileged pharmacophoric features for binding to protein kinases (Bamborough *et al.*, 2011), but none has previously been reported to bind to Erk-2. We describe their interactions with the protein in some detail. Notably, these fragments showed no detectable inhibition when tested at 0.1 m*M* and limited or no stabilization of the protein kinase in a thermal shift assay. Only a small shift of the melting temperature

(∼0.6°C at concentrations of 0.5 and 1 m*M*) is detected for compound **4** (while reference compounds showing micromolar inhibition yielded a significant shift of 2°C in the same conditions).

In the cases of 2-amino-6-thiopurine (**1**; molecular weight 167, *X*log*P* 0.13) and diaminophenyltriazole (**2**; molecular weight 175, *X*log*P* 0.65), three structures were solved independently for each ligand using data sets recorded (i) at RT on a laboratory anode (using 7–8 crystals), (ii) at RT on BM30A (3–4 crystals) and (iii) at 100 K (one crystal). To obtain an optimal resolution, data were recorded using 3 min oscillations of 1° per image on the rotating-anode generator. This led to significant radiation damage, limiting the range of useful data and therefore requiring a larger number of crystals to obtain a complete data set. The various data sets were merged on-the-fly to stop collecting data as soon as an acceptable completeness had been achieved.

In all cases, a clear density was observed in the vicinity of the hinge, as expected (see Supplementary Figs. S4 and Fig. 3 for ligands **1** and **2**, respectively), and the ligands were unambiguously placed before completing the refinement and gave very good statistics (Table 2). These results were confirmed by running the *phenix.ligand_pipeline* routine in *PHENIX* (Echols *et al.*, 2014). In all cases, the ligand was detected with default parameters and good overall statistics (CC ranging from 0.88 to 0.95 for the data collected at RT). The amino groups and the attached heterocyclic moiety of both compounds interact with the protein hinge (residues Glu104 and Met106) through a network of hydrogen bonds. In parallel, the aromatic rings are sandwiched by three conserved hydrophobic residues: Val37, Ala50 and Leu154. In the case of compound **1**, the catalytic residue Lys52 is attracted towards the ligand and forms a weak hydrogen bond to an N atom of the purine ring (N7). This configuration is stabilized by the gatekeeper residue Gln103, which also forms a hydrogen bond to the terminal N atom of the catalytic lysine.

Another fragment, an azaindole (**3**; molecular weight 143, *X*log*P* 1.29), was then tested on Erk-2 (Table 3 and Fig. 4*a*). In this case, we only compared the results of *in situ* diffraction recorded on the rotating-anode generator and diffraction using a cooled crystal on beamline ID23-2. To limit radiation damage, we reduced the exposure time to 2 min per image (1° rotation). This led us to record an 88% complete data set using only two distinct crystals at the expense of the resolution (2.55 Å). Despite the lower resolution, the ligand could be readily recognized in the extra density observed near the hinge as in the case of compounds **1** and **2**. However, in this case, the map correlation computed by *phenix.ligand_pipeline* was slightly lower (CC = 0.77). Compound **3** crystallized during solvent evaporation, but this did not preclude its subsequent diffusion into the protein crystal (Figs. 1*b*, 4*b*, 4*c* and 4*d*).

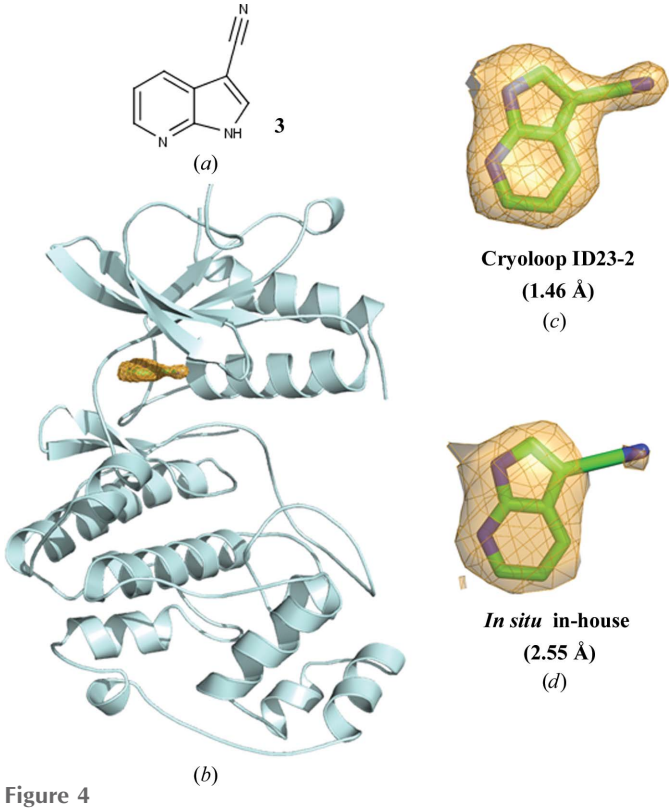

Figure 4
Crystal structures of the protein kinase Erk-2 in complex with 3-cyano-7-azaindole (**3**). (*a*) Chemical structure of compound **3**. (*b*) The overall structure of Erk-2 shown as a cartoon representation. (*c*) Structure solved at high resolution at 100 K. (*d*) The same structure at RT using data collected on a rotating-anode generator. In all panels the $2F_o - F_c$ electron-density map (contoured at 1σ) was computed with the ligand molecule omitted in the Fourier synthesis.

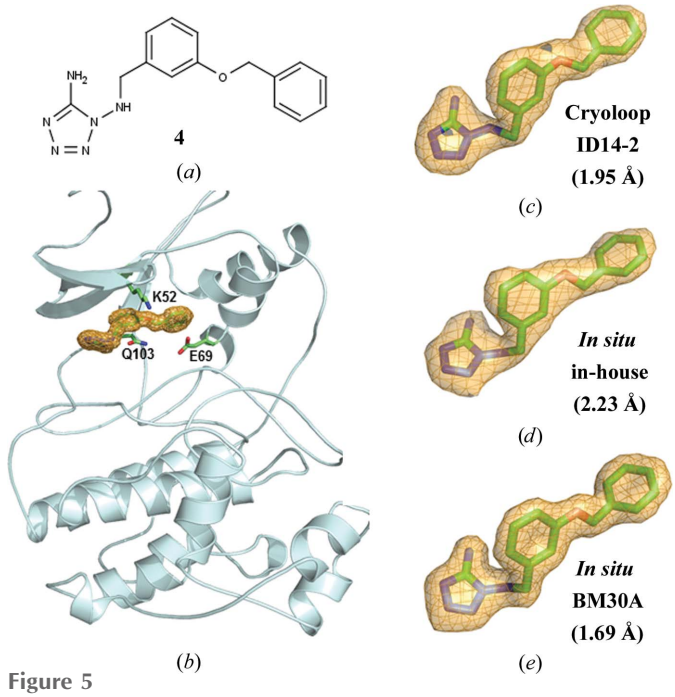

Figure 5
In cristallo screening. Crystal structures of the protein kinase Erk-2 in complex with the new binder **4**. (*a*) The chemical structure of compound **4**. (*b*) The overall structure of Erk-2 shown as a cartoon representation with key residues shown in stick representation. (*c*) Structure solved at high resolution at 100 K. (*d*) The same structure at RT using data collected on a rotating-anode generator. (*e*) The same structure at RT using data collected on the synchrotron beamline BM30A at ESRF. In all panels the $2F_o - F_c$ electron-density map (contoured at 1σ) was computed with the ligand molecule omitted in the Fourier synthesis.

For all of these compounds, their binding mode and their interactions with the protein matched those usually observed for similar ligands in protein kinases. Indeed, the binding mode of 2-amino-6-thiopurine (**1**) was highly similar to that adopted by a bromophenyl derivative of 2-aminopurine previously shown to bind to Erk-2 with micromolar affinity (PDB entry 3qyw; le Maire *et al.*, 2011). The diaminotriazole moiety of **2** mimics the 2-aminopurine moiety of **1** and is likely to represent the portion interacting with the protein hinge in a large series of related chemical compounds patented as potent protein kinase inhibitors by Vertex Inc. (US Patent 7902239 B2). This suggests that our fragment screening would have identified new binders suitable for further elaboration into better compounds.

We also tested a larger and more flexible ligand, 1-*N*-{[3-(benzyloxy)phenyl]methyl}-2*H*-1,2,3,4-tetrazole-1,5-diamine (**4**; molecular weight 296, *X*log*P* 3.54), which had not previously been described as a protein kinase inhibitor (Fig. 5*a*). Again, we could rapidly detect the bound ligand (Figs. 5*b*, 5*c* and 5*d*) using data recorded at RT on a rotating-anode generator (seven crystals), at RT on BM30A (two crystals) and at 100 K (one crystal) (Table 3). In this case, an automatic ligand search yielded high correlation coefficients for data sets both recorded *in situ* on the rotating-anode generator and on the synchrotron beamline BM30A (CC of 0.85 and 0.94, respectively). The diaminotetrazole moiety interacted with the protein hinge, as did the equivalent moiety of compound **2** (described above). Surprisingly, the central phenyl ring is sandwiched between the catalytic residue Lys52 and the gatekeeper Gln103, while the terminal benzyl moiety pointed deeply into the protein core towards α-helix C and was stacked onto the side chain of the glutamate Glu69 (Fig. 5*b*). Accordingly, this compound induced a significant rearrangement of the ATP-binding site upon binding to access a buried subpocket that had not previously been described. This may open up a new route towards higher specificity of ligands targeting Erk-2.

A survey of the PDB (Rose *et al.*, 2011) highlighted that various other protein kinases (for example, KIT, TGFBR1, JAK2 and EPHB4 among the tyrosine kinases and CDK2, CHK1, PLK4 and PI3K among the serine/threonine kinases) already give rise to decent X-ray diffraction on a rotating-anode generator, suggesting that these important therapeutic targets are also amenable to this approach for the development of new drugs.

4. Discussion

In this study, we have further developed the technique of precoating of crystallization plates with small molecules in order to accelerate ligand screening using X-ray crystallography. In summary, co-crystallization with dried ligands was successfully tested using several relevant therapeutic targets. The major limitation comes from the limited reproducibility of protein crystal growth despite the use of microseeding. As mentioned previously (Newman *et al.*, 2009), microseeding depends on a delicate balance between obtaining too many tiny crystals, a few large crystals and no crystals at all. As observed here, this step still represents the bottleneck on the way to fully automatic screening by X-ray crystallography. Nevertheless, when co-crystallization did occur, we could straightforwardly identify the bound ligands in the computed $F_o - F_c$ maps. In the case of the protein kinase Erk-2, our study brought to light new complexes that may be useful for further derivation of potent inhibitors. Some sulfate ions could be detected on the protein surface of Erk-2, but no DMSO molecules. This is in marked contrast to the same structures solved from cooled crystals soaked with fragments solubilized in this solvent. As DMSO can deteriorate protein crystals, its absence after evaporation opens new opportunities for screening by X-ray crystallography. Accordingly, with this technique in hand, most chemical libraries are now amenable to automatic dispensing prior to co-crystallization with targeted macromolecules.

The combination with *in situ* diffraction alleviates the requirement for crystal manipulation and cooling. In this case, direct X-ray data collection can be performed in ~2 h on a rotating-anode generator or in ~10 min on a bending magnet (BM30A) and one crystal is usually sufficient (except for triclinic and monoclinic space groups, which represent ~30% of the observed lattices in protein crystals). The recent development of ultrarapid detectors (Owen *et al.*, 2014) and high-brilliance X-ray beams (Axford *et al.*, 2012) may decrease this duration to a few seconds, while possibly extending the range of data that one can collect from a single crystal. Currently, there are already six distinct beamlines equipped for *in situ* data-set collections, and the proposed ligand-deposition methodology can be rapidly disseminated as it relies solely on the use of widely distributed liquid dispensers.

Thus, the proposed method of *in situ* 'dry' co-crystallization provides an ideal way to accelerate and automate ligand screening by X-ray crystallography. A combination of 'dry' co-crystallization with on-chip serial crystallography (Heymann *et al.*, 2014) may also be considered in order to develop an alternative automation procedure for ligand screening in the case of macromolecular crystals that are too fragile to sustain (even a partial) data collection. In this case, a shower of crystals would become exploitable and this may represent an attractive solution to the problem of massive crystal growth reproduction.

Acknowledgements

The authors acknowledge financial support from the CEA, CNRS, INSERM, Université Montpellier, Région Languedoc-Roussillon ('Chercheur d'Avenir') and the ANRS (AO2012-2). MG was awarded a grant by the INCa (INCA 2010-083). This work was supported by the French Infrastructure for Integrated Structural Biology (FRISBI) ANR-10-INSB-05-01. We would like to thank Dr M. Cobb for the gift of the Erk-2 plasmid and Dr D. Schlatter for the gift of the cyclophilin D plasmid. We wish to thank Dr M. Cohen-Gonsaud for helpful discussion and the referees for valuable comments. We wish to acknowledge the help from people at the various beamlines at the ESRF in Grenoble, France. As a conflict of interest, we

have to mention that J-LF is a co-founder of the NatX-ray company (http://www.natx-ray.com/) and is a member of its scientific advisory board.

References

Adams, P. D. *et al.* (2010). *Acta Cryst.* D**66**, 213–221.
Ahmadian, M., Suh, J. M., Hah, N., Liddle, C., Atkins, A. R., Downes, M. & Evans, R. M. (2013). *Nature Med.* **19**, 557–566.
Alam, M. R., Baetz, D. & Ovize, M. (2015). *J. Mol. Cell. Cardiol.* **78**, 80–89.
Axford, D., Foadi, J., Hu, N.-J., Choudhury, H. G., Iwata, S., Beis, K., Evans, G. & Alguel, Y. (2015). *Acta Cryst.* D**71**, 1228–1237.
Axford, D. *et al.* (2012). *Acta Cryst.* D**68**, 592–600.
Baker, M. (2013). *Nature Rev. Drug Discov.* **12**, 5.
Bamborough, P., Brown, M. J., Christopher, J. A., Chung, C.-W. & Mellor, G. W. (2011). *J. Med. Chem.* **54**, 5131–5143.
Bingel-Erlenmeyer, R., Olieric, V., Grimshaw, J. P. A., Gabadinho, J., Wang, X., Ebner, S. G., Isenegger, A., Schneider, R., Schneider, J., Glettig, W., Pradervand, C., Panepucci, E. H., Tomizaki, T., Wang, M. & Schulze-Briese, C. (2011). *Cryst. Growth Des.* **11**, 916–923.
Cipriani, F., Röwer, M., Landret, C., Zander, U., Felisaz, F. & Márquez, J. A. (2012). *Acta Cryst.* D**68**, 1393–1399.
Cymborowski, M., Klimecka, M., Chruszcz, M., Zimmerman, M. D., Shumilin, I. A., Borek, D., Lazarski, K., Joachimiak, A., Otwinowski, Z., Anderson, W. & Minor, W. (2010). *J. Struct. Funct. Genomics*, **11**, 211–221.
Davies, D. R. (2014). *Methods Mol. Biol.* **1140**, 315–323.
Davies, D. R., Mamat, B., Magnusson, O. T., Christensen, J., Haraldsson, M. H., Mishra, R., Pease, B., Hansen, E., Singh, J., Zembower, D., Kim, H., Kiselyov, A. S., Burgin, A. B., Gurney, M. E. & Stewart, L. J. (2009). *J. Med. Chem.* **52**, 4694–4715.
Delfosse, V., Grimaldi, M., Pons, J.-L., Boulahtouf, A., le Maire, A., Cavailles, V., Labesse, G., Bourguet, W. & Balaguer, P. (2012). *Proc. Natl Acad. Sci. USA*, **109**, 14930–14935.
Echols, N., Moriarty, N. W., Klei, H. E., Afonine, P. V., Bunkóczi, G., Headd, J. J., McCoy, A. J., Oeffner, R. D., Read, R. J., Terwilliger, T. C. & Adams, P. D. (2014). *Acta Cryst.* D**70**, 144–154.
Emsley, P., Lohkamp, B., Scott, W. G. & Cowtan, K. (2010). *Acta Cryst.* D**66**, 486–501.
Guichou, J.-F., Colliandre, L., Ahmed-Belkacem, H. & Pawlotsky, J.-M. (2011). Patent WO/2011/076784.
Heymann, M., Opthalage, A., Wierman, J. L., Akella, S., Szebenyi, D. M. E., Gruner, S. M. & Fraden, S. (2014). *IUCrJ*, **1**, 349–360.
Jacquamet, L., Ohana, J., Joly, J., Borel, F., Pirocchi, M., Charrault, P., Bertoni, A., Israel-Gouy, P., Carpentier, P., Kozielski, F., Blot, D. & Ferrer, J.-L. (2004). *Structure*, **12**, 1219–1225.
Kabsch, W. (2010). *Acta Cryst.* D**66**, 125–132.
Kofron, J.-L., Kuzmic, P., Kishore, V., Colon-Bonilla, E. & Rich, H. (1991). *Biochemistry*, **25**, 6127–6134.
Maire, A. le, Gelin, M., Pochet, S., Hoh, F., Pirocchi, M., Guichou, J.-F., Ferrer, J.-L. & Labesse, G. (2011). *Acta Cryst.* D**67**, 747–755.
Michalik, L. *et al.* (2006). *Pharmacol. Rev.* **58**, 726–741.
Moriarty, N. W., Grosse-Kunstleve, R. W. & Adams, P. D. (2009). *Acta Cryst.* D**65**, 1074–1080.
Murray, C. W. & Blundell, T. L. (2010). *Curr. Opin. Struct. Biol.* **20**, 497–507.
Murshudov, G. N., Skubák, P., Lebedev, A. A., Pannu, N. S., Steiner, R. A., Nicholls, R. A., Winn, M. D., Long, F. & Vagin, A. A. (2011). *Acta Cryst.* D**67**, 355–367.
Newman, J., Fazio, V. J., Caradoc-Davies, T. T., Branson, K. & Peat, T. S. (2009). *J. Biomol. Screening*, **14**, 1245–1250.
Nolte, R. T., Wisely, G. B., Westin, S., Cobb, J. E., Lambert, M. H., Kurokawa, R., Rosenfeld, M. G., Willson, T. M., Glass, C. K. & Milburn, M. V. (1998). *Nature (London)*, **395**, 137–143.
Owen, R. L., Paterson, N., Axford, D., Aishima, J., Schulze-Briese, C., Ren, J., Fry, E. E., Stuart, D. I. & Evans, G. (2014). *Acta Cryst.* D**70**, 1248–1256.
Powell, H. R., Johnson, O. & Leslie, A. G. W. (2013). *Acta Cryst.* D**69**, 1195–1203.
Rose, P. W., Beran, B., Bi, C., Bluhm, W. F., Dimitropoulos, D., Goodsell, D. S., Prlic, A., Quesada, M., Quinn, G. B., Westbrook, J. D., Young, J., Yukich, B., Zardecki, C., Berman, H. M. & Bourne, P. E. (2011). *Nucleic Acids Res.* **39**, D392–D401.
Schüttelkopf, A. W. & van Aalten, D. M. F. (2004). *Acta Cryst.* D**60**, 1355–1363.
Tanley, S. W. M., Schreurs, A. M. M., Kroon-Batenburg, L. M. J., Meredith, J., Prendergast, R., Walsh, D., Bryant, P., Levy, C. & Helliwell, J. R. (2012). *Acta Cryst.* D**68**, 601–612.
Tontonoz, P. & Spiegelman, B. M. (2008). *Annu. Rev. Biochem.* **77**, 289–312.
Varga, T., Czimmerer, Z. & Nagy, L. (2011). *Biochim. Biophys. Acta*, **1812**, 1007–1022.
Winn, M. D. *et al.* (2011). *Acta Cryst.* D**67**, 235–242.
Wortzel, I. & Seger, R. (2011). *Genes Cancer*, **2**, 195–209.
Yin, X., Scalia, A., Leroy, L., Cuttitta, C. M., Polizzo, G. M., Ericson, D. L., Roessler, C. G., Campos, O., Ma, M. Y., Agarwal, R., Jackimowicz, R., Allaire, M., Orville, A. M., Sweet, R. M. & Soares, A. S. (2014). *Acta Cryst.* D**70**, 1177–1189.
Zhang, H., Xu, X., Chen, L., Chen, J., Hu, L., Jiang, H. & Shen, X. (2011). *PLoS One*, **6**, e28253.